Journal of Sound and Vibration (1997) **204**(2), 213–237

VIBRATION AND NOISE GENERATION BY ELASTIC ELEMENTS EXCITED BY A TURBULENT FLOW

A. O. Borisyuk and V. T. Grinchenko

Institute of Hydromechanics of the National Academy of Sciences of Ukraine, Zhelyabova Street 8/4, 252680 *Kiev*-57 *MSP, Ukraine*

(*Received* 24 *February* 1995, *and in final form* 8 *January* 1997)

Vibration and sound generation by elastic structural elements (membrane, strip and plate) of streamlined surfaces excited by low Mach number turbulent flow is considered. The models of Corcos, Chase, Ffowcs Williams and Smol'yakov-Tkachenko for the wavenumber-frequency spectrum of the wall pressure field beneath a turbulent boundary layer are used to describe random excitation. A comparative analysis of the models is carried out. The Chase and Smol'yakov-Tkachenko models are shown to have the best agreement with the Martin and Leehey experimental data. The differences in the predictions of sound fields of turbulence excited elastic elements for all the above models are demonstrated and analyzed. The roles of the acoustic, low wavenumber, and convective wall pressure components are studied. The convective components are shown to make a significant contribution to the vibration and acoustic fields produced by turbulence. The ranges of parameters of the flow and the elastic structure are found (away from structural resonances) where the differences between the wall pressure models are not important for predictions of the sound radiated. At the same time these differences are important when the sound field is estimated near structural resonances.

1. INTRODUCTION

Noise produced by elastic bodies moving through low Mach number turbulent flows has been and is still of interest in many engineering applications. This problem can be treated as sound radiation from the forced vibrations of elastic structural elements in the acoustic medium, the choice of the pressure fluctuation field model on the rigid wall being in fact the choice of the model for the excitation forces (hypothesis of "blocked pressure" [1, 2]). However, in solving many practically important aspects of this problem there are considerable difficulties connected with modelling of boundary layer wall pressures.

At present there are several empirical and semiempirical models for the rigid wall pressure fluctuation field beneath an incompressible turbulent boundary layer. The first of these was proposed by Corcos [3]. It was devised to describe the surface pressure field on hydroacoustic transducers flush-mounted in a streamlined surface under a turbulent boundary layer. In this case the energy of the turbulent boundary layer is governed by the convective components. As a result, the Corcos model describes quite well the structure of the wavenumber–frequency spectrum of the wall pressure, $\Phi_p(k_1, k_2, \omega)$ only in the range of the convective wavenumber, $k_1 \approx k_c = \omega/U_c$, where $\Phi_p(k_1, k_2, \omega)$ is sharply peaked, owing to the convected nature of the turbulence (see Figure 1). However, spectral levels at wavenumbers below the convective peak, $k_1 \ll k_c$, are considerably overpredicted by the

0022–460X/97/270213 + 25 $25.00/0/sv970920

model [1, 4]. If one is interested in the acoustic far field then it is clear, at any rate qualitatively, that the wall pressure long wavelength subconvective components (viz. acoustic components, $k_1 < k_0 = \omega/c_0$, and low-wavenumber components, $k_0 < k_1 \ll k_c$) should play a dominant role, and to make calculations it is necessary to have other models. Their construction is very difficult mainly for two reasons. Firstly, it is very difficult to carry out an experiment aimed at directly measuring the long wavelength components. Secondly, it is necessary to take into account the quadratic decrease of the wavenumber-frequency spectrum at low wavenumbers in such models. The decrease is predicted by the Phillips–Kraichnan theory [1, 5, 6], which has recently been confirmed by Howe [7].

More recent models by Chase [8], Ffowcs Williams [9] and Smol'yakov-Tkachenko [10] have been designed to describe the low-wavenumber range. All of them approximate the convective domain of the spectrum equally well, but they differ from each other in both acoustic and low wavenumber ranges. These differences raise questions about comparisons of the models and determination of their relative advantages and disadvantages, as well as the limits of their application. However, only a rather restricted number of works have been reported which treat this problem [1, 10–12]. In addition, the authors of those works do not consider all the models simultaneous, and they also use both different conditions and different ranges of parameters. Consequently, the results obtained and corresponding conclusions made by them are restricted to those conditions and parameters, and, therefore, they cannot be applied to each situation studied. This stimulates interest in making a new comparison of the above wall pressure models in order to determine which of them are preferable for theoretical predictions of fields generated by low Mach number turbulence for the conditions of particular interest. This comparison is one of the aims of this paper.

Most previous investigations of the turbulent energy re-emitted by elastic bodies in a low Mach number flow are based on the use of the Corcos model. Within its limits, fixed ratios between the spectral levels of the different wall pressure components have been determined, the spectral levels of the long wavelength components being 25–35 dB higher than the available experimental data [1, 4]. This results not only in errors in estimating the radiated sound characteristics, but also results in distortion of the role of the different excitation force components in the fields generated by a turbulent flow. In particular, this permits the neglect of the contribution from the energy containing convective components in those fields. Apart from other consequences, this is associated with the neglect of acoustic scattering of subsonic surface waves, excited by those components, into sound at structural inhomogeneities. This acoustic scattering (which, in terms of the wavenumber-frequency spectrum, $\Phi_p(k_1, k_2, \omega)$, can be interpreted as the transformation of the

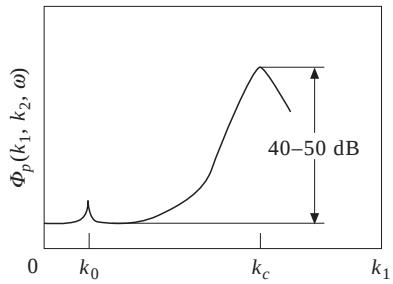

Figure 1. Wavenumber–frequency spectrum $\Phi_p(k_1, k_2, \omega)$ of turbulent wall pressure with $k_2 = const$, $\omega = const$.

turbulence energy from the energy-containing pseudosound convective domain to the acoustically efficient low wavenumber and acoustic domains) can be an important contributor to the total noise field produced by turbulence [13]. In connection with this the use of other turbulent pressure field models (in which the ratio between the spectral levels of the convective and subconvective components has been changed) will, thus, permit one to (1) obtain more correct estimates of the vibration and acoustic field characteristics; and (2) determine the contribution from the different wall pressure components in those fields more correctly, and, therefore, probably take into account the energy conversion process at structural inhomogeneities. These questions are also considered in this work.

This paper commences with a brief description of the incompressible turbulent wall pressure models (section 2), which are then compared with the experimental data by Martin and Leehey [4] (section 3). Section 4 presents the simple one dimensional model problems which qualitatively illustrate the roles of the different wall pressure components in the turbulent energy re-emitted by elastic elements near and away from structural resonances, all the models for $\Phi_p(k_1, k_2, \omega)$ being considered. In section 5 a simply supported thin rectangular elastic plate inserted in an infinite rigid baffle and turbulent boundary layer excited on one side is considered, and the differences in the radiated sound power spectral density are analyzed. These differences are due to the different models developed for the wavenumber-frequency spectrum of the pressure fluctuation field.

Finally, the conclusions of the investigation are summarized in section 6, and a list of symbols is given in the Appendix.

2. TURBULENT WALL PRESSURE MODELS

A random turbulent wall pressure field, $p_t(x_1, x_2, t)$, on a plane streamlined surface is described in terms of its statistical characteristics, such as the cross-correlation function, cross-spectral density, power (or frequency) spectrum, and wavenumber-frequency spectrum. With the wall pressure field assumed to be spatially homogeneous and temporally stationary, the space-time cross-correlation function of the pressure at two arbitrary space-time points (x_1, x_2) and t, and $(x_1 + \xi_1, x_2 + \xi_2)$ and $t + \tau$ is written as

$$R_p(\xi_1, \xi_2, \tau) = \langle p_t(x_1, x_2, t) p_t(x_1 + \xi_1, x_2 + \xi_2, t + \tau) \rangle, \tag{1}$$

where the brackets $\langle\ \rangle$ denote an ensemble average. The cross spectrum $S_p(\xi_1, \xi_2, \omega)$ and correlation function $R_p(\xi_1, \xi_2, \tau)$ are a pair of Fourier transforms,

$$S_p(\xi_1, \xi_2, \omega) = (1/2\pi) \int_{-\infty}^{\infty} R_p(\xi_1, \xi_2, \tau)\, \mathrm{e}^{\mathrm{i}\omega\tau}\, \mathrm{d}\tau,$$

$$R_p(\xi_1, \xi_2, \tau) = \int_{-\infty}^{\infty} S_p(\xi_1, \xi_2, \omega)\, \mathrm{e}^{-\mathrm{i}\omega\tau}\, \mathrm{d}\omega, \tag{2}$$

and the wavenumber-frequency spectrum $\Phi_p(k_1, k_2, \omega)$ is obtained from $R_p(\xi_1, \xi_2, \tau)$ by taking the Fourier transform over space and time, i.e.,

$$\Phi_p(k_1, k_2, \omega) = (1/2\pi)^3 \int_{-\infty}^{\infty} \int_{-\infty}^{\infty} \int_{-\infty}^{\infty} R_p(\xi_1, \xi_2, \tau)\, \mathrm{e}^{-\mathrm{i}(k_1\xi_1 + k_2\xi_2 - \omega\tau)}\, \mathrm{d}\xi_1\, \mathrm{d}\xi_2\, \mathrm{d}\tau. \tag{3}$$

The cross-spectral density $S_p(\xi_1, \xi_2, \omega)$ reduces to the frequency spectrum $P(\omega)$ for $\xi_1 = 0$, $\xi_2 = 0$, i.e.,

$$P(\omega) = S_p(0, 0, \omega) = (1/2\pi) \int_{-\infty}^{\infty} R_p(0, 0, \tau)\, e^{i\omega\tau}\, d\tau, \tag{4}$$

and, since $S_p(\xi_1, \xi_2, \omega)$ and $\Phi_p(k_1, k_2, \omega)$ are related by the expressions

$$\Phi_p(k_1, k_2, \omega) = (1/2\pi)^2 \int_{-\infty}^{\infty} \int_{-\infty}^{\infty} S_p(\xi_1, \xi_2, \omega)\, e^{-i(k_1\xi_1 + k_2\xi_2)}\, d\xi_1\, d\xi_2,$$

$$S_p(\xi_1, \xi_2, \omega) = \int_{-\infty}^{\infty} \int_{-\infty}^{\infty} \Phi_p(k_1, k_2, \omega)\, e^{i(k_1\xi_1 + k_2\xi_2)}\, dk_1\, dk_2, \tag{5}$$

obviously

$$P(\omega) = \int_{-\infty}^{\infty} \int_{-\infty}^{\infty} \Phi_p(k_1, k_2, \omega)\, dk_1\, dk_2. \tag{6}$$

Modelling of a turbulent wall pressure has been a subject for many years, but at the present time no explicit model is available for the full wavenumber-frequency spectrum of wall pressure fluctuations beneath a turbulent boundary layer. Following Corcos [3], one can write the cross-spectrum of a stationary and homogeneous wall pressure field in a separable form as

$$S_p(\xi_1, \xi_2, \omega) = P(\omega)A(\omega\xi_1/U_c)B(\omega\xi_2/U_c)\, e^{-i\omega\xi_1/U_c}. \tag{7}$$

In practice [1, 3], $A(\omega\xi_1/U_c)$ and $B(\omega\xi_2/U_c)$ are frequently approximated by exponential decay functions,

$$S_p(\xi_1, \xi_2, \omega) = P(\omega)\, e^{-\beta_1|\omega\xi_1/U_c|}\, e^{-\beta_2|\omega\xi_2/U_c|}\, e^{-i\omega\xi_1/U_c}, \tag{8}$$

where β_1 and β_2 are parameters chosen to yield the best agreement with experiment. Substituting equation (8) into equation (5) and performing the Fourier transform yields the Corcos model for the turbulent wall pressure wavenumber-frequency spectrum:

$$\Phi_p(k_1, k_2, \omega) = P(\omega)\beta_1\beta_2/\pi^2[(k_1U_c/\omega - 1)^2 + \beta_1^2][(k_2U_c/\omega)^2 + \beta_2^2]. \tag{9}$$

This model continues to be widely used at the present time. The usual justification is that the mathematics are simple and of closed form. However, the use of equation (9) provides satisfactory results only when k_1 is in the neighbourhood of the convective wavenumber, $k_c = \omega/U_c$. When k_1 is in the subconvective range, $k_1 \ll k_c$, expression (9) tends to overpredict significantly (25–35 dB) the subconvective spectrum [1, 4]. Also, it violates the $|k|^2 = k_1^2 + k_2^2$ dependence of the low-wavenumber spectrum as $|k|$ approaches zero.

In contrast to Corcos, who constructed his model based on an examination of published experimental data, Chase [8] and Ffowcs Williams [9] used analytical or quasi-analytical approaches in attempts to describe the subconvective region more accurately.

Chase [8] considered contributions of both mean shear and pure turbulence to the spectrum of the wall pressure, and obtained the following mathematical model for $\Phi_p(k_1, k_2, \omega)$:

$$\Phi_p(k_1, k_2, \omega) = \rho_0^2 v_*^3[c_M k_1^2 K_M^{-5} + c_T(k_1^2 + k_2^2)K_T^{-5}],$$
$$K_i^2 = (\omega - U_c k_1)^2/(h_i v_*)^2 + (k_1^2 + k_2^2) + (b_i\delta)^{-2}, \qquad i = M, T. \tag{10}$$

With the dimensionless coefficients $h_M \approx h_T \approx 3$, $c_T = 0{\cdot}0474$, $c_M = 0{\cdot}0745$, $b_T = 0{\cdot}378$ and $b_M = 0{\cdot}756$, recommended by Chase, equation (10) can predict a convective pressure level

which agrees well with that measured in wind tunnels, and the wavenumber spectrum displays the $|k|^2$ dependence in the low-wavenumber domain.

Starting from Lighthill's acoustic analogy [14, 15], and assuming that the velocity source terms were of the general Corcos form, Ffowcs Williams [9] derived the following expression for $\Phi_p(k_1, k_2, \omega)$:

$$\Phi_p(k_1, k_2, \omega) = \rho_0^2 U_\infty^3 \Delta^3 \Phi_0(\omega\Delta/U_\infty) A_0(1 - k_1 U_c/\omega) B_0(k_2 U_c/\omega) \times (a_0(U_\infty(k_1^2 + k_2^2)^{1/2}/\omega)^2 + a_1 M^2 + a_2 M^4 \ln(R/\Delta)\delta[(U_\infty(k_1^2 + k_2^2)^{1/2}/\omega)^2 - M^2]). \quad (11)$$

This contains unknown constants a_0, a_1, a_2 and functions Φ_0, A_0, B_0 to be determined experimentally. To date, these constants and functions remain unknown, but Hwang and Geib [11] have proposed a simplified version, in which the effects of compressibility are neglected and a specific form is assumed for the remaining functions; their expression, slightly adjusted to agree with the Corcos parameters, is

$$\Phi_p(k_1, k_2, \omega) = P(\omega)[(k_1^2 + k_2^2)^{1/2} U_c/\omega]^2 \frac{\beta_1\beta_2\pi^{-2}}{[(k_1 U_c/\omega - 1)^2 + \beta_1^2][(k_2 U_c/\omega)^2 + \beta_2^2]}. \quad (12)$$

It also has the $|k|^2$ dependence in the low-wavenumber range.

More recently, a refined version of the Corcos approach has also appeared [10]. Smol'yakov and Tkachenko measured cross-spectral densities as a function of spatial separation and boundary layer thickness, and fitted exponential curves to their results. However, in contrast to Corcos, who directly multiplied his pure longitudinal and pure lateral cross-spectra, giving expressions (7) and (8), they took the combined cross-spectrum to be of the form $\exp[-((\beta_1|\omega\xi_1/U_c|)^2 + (\beta_2|\omega\xi_2/U_c|)^2)^{1/2}]$, and Fourier transformed this expression. The final expression of their wavenumber–frequency spectrum is

$$\Phi_p(k_1, k_2, \omega) = 0{\cdot}025P(\omega)A(\omega)h(\omega)(U_c/\omega)^2[F(k_1, k_2, \omega) - \Delta F(k_1, k_2, \omega)],$$

$$A(\omega) = 0{\cdot}124[1 - 0{\cdot}2/\omega^* + (0{\cdot}2/\omega^*)^2]^{1/2}, \qquad \omega^* = \omega\delta^*/U_\infty,$$

$$F(k_1, k_2, \omega) = [A^2 + (1 - U_c k_1/\omega)^2 + 0{\cdot}024(U_c k_2/\omega)^2]^{-3/2},$$

$$\Delta F(k_1, k_2, \omega) = 0{\cdot}995[A^2 + 1 + (1{\cdot}005/m_1)[(m_1 - U_c k_1/\omega)^2 + (U_c k_2/\omega)^2 - m_1^2]]^{-3/2},$$

$$m_1 = (A^2 + 1)/(1{\cdot}025 + A^2),$$

$$h(\omega) = [1 - 0{\cdot}153A(A^2 + 1)/((1{\cdot}025 + A^2)(0{\cdot}02 + A^2))^{1/2}]^{-1}. \quad (13)$$

Although Smol'yakov and Tkachenko gave arguments and reported experimental results supporting their model, expression (13) violates the $|k|^2$ behaviour of the spectrum $\Phi_p(k_1, k_2, \omega)$ at low wavenumbers.

3. COMPARISON OF MODELS

In this section the Chase, Ffowcs Williams, and Smol'yakov-Tkachenko models (given by expressions (10), (12) and (13), respectively) are compared in order to determine which of them are preferable for theoretical predictions of vibration and acoustic fields of elastic elements excited by low Mach number turbulent flow. The results of the experimental work by Martin and Leehey [4] are used herewith. The Corcos model (9) is not considered in this section, because it is obvious that this model will significantly overpredict the reference data.

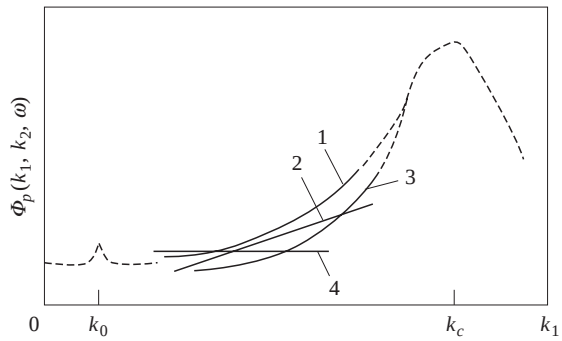

Figure 2. Possible result of comparison of models for wavenumber–frequency spectrum $\Phi_p(k_1, k_2, \omega)$ with $k_2 = 0$, $\omega = const$: 1, Ffowcs Williams model ($\Phi_p \sim \gamma_3 k_1^2$); 2, Smol'yakov–Tkachenko model ($\Phi_p \sim \gamma_4 k_1$); 3, Chase model ($\Phi_p \sim \gamma_2 k_1^2$); 4, Martin-Leehey model ($\Phi_p = \gamma_1 k_1^{0.03}$).

From the very beginning one needs to decide which method of comparison should be used, and what experimental data should be taken as the corresponding reference data. The usual method is based on comparison of theoretical and experimental curves of function $\Phi_p(k_1, k_2, \omega)$, and the resulting conclusion about the advantage of one model over the other model is made from better agreement between the model theoretical curves and experimental curve. However, the following reasons makes this approach inapplicable here. On the one hand, the Martin–Leehey approximation of the low wavenumber-frequency spectrum $\Phi_p(k_1, 0, \omega)$ (their work is one of the most complete, accurate and most cited among similar studies available) expresses $\gamma_1 k_1^{0.03}$ dependence, which is in contrast to that predicted by the Phillips–Kraichnan theory [1, 5, 6]. On the other hand, the low-wavenumber behaviour of the spectra (10), (12), and (13) is different, viz, Chase spectrum $\Phi_p(k_1, 0, \omega) \sim \gamma_2 k_1^2$, Ffowcs Williams spectrum, $\Phi_p(k_1, 0, \omega) \sim \gamma_3 k_1^2$, Smol'yakov–Tkachenko spectrum, $\Phi_p(k_1, 0, \omega) \sim \gamma_4 k_1$, and the behaviour does not agree with that given by Martin and Leehey (here the γ_i are different functions of frequency, boundary layer thickness, etc.; $\partial\gamma_i/\partial k_1 = 0$, $i = 1, \ldots, 4$). In such a situation direct comparison of these theoretical and experimental curves $\Phi_p(k_1, 0, \omega)$ can result in rather questionable conclusions, because (1) if one considers the Martin–Leehey data to be accurate then the principally different behaviour of both the theoretical and experimental spectra will not allow one to determine exactly which of the models come out best in the model comparison (a possible result of the comparison is shown in Figure 2), and (2) if the Martin–Leehey data are assumed to be incorrect then the conclusions made from the comparison of the theoretical curves with the inaccurate experimental curve will be incorrect.

Taking into account the arguments presented one comes to the necessity of using the other way of comparison which was developed in the authors' previous work [16, 17]. The basic idea of that method is to compare the predictions of turbulence induced fields in the framework of the different models with those measured experimentally, and thereby to assess the applicability of the wall pressure models to the problems of flow-induced noise and vibration. The main advantage of this approach over that discussed above is that it is much more easy to measure correctly the characteristics of fields produced by turbulence than measure the characteristics of the turbulent wall pressure. Therefore, the reference data used in our method will be much more truthful than those used in previous method.

To proceed from this idea, one considers a turbulent-wall-pressure-excited uniform rectangular membrane as used by Martin and Leehey in their experiments [4]. The simply supported membrane has streamwise and lateral dimensions l_1 and l_2, respectively, mass

per unit area m_s, and uniform tensile force per unit length T. The random turbulent pressure field $p_t(x_1, x_2, t)$ is assumed to be time-stationary and homogeneous. The membrane motion, subjected to a damping force per unit mass $\beta\partial w/\partial t$, is governed by the equation for the normal displacement $w(x_1, x_2, t)$,

$$\frac{\partial^2 w}{\partial t^2} + \beta\frac{\partial w}{\partial t} - \frac{T}{m_s}\left(\frac{\partial^2 w}{\partial x_1^2} + \frac{\partial^2 w}{\partial x_2^2}\right) = -p_t(x_1, x_2, t)/m_s, \tag{14}$$

with the corresponding boundary conditions

$$w|_{x_1 = 0, l_1} = w|_{x_2 = 0, l_2} = 0. \tag{15}$$

Following the Martin–Leehey analysis, one can write the displacement response spectral density in the form of a sum of contributions from the *in vacuo* membrane normal modes $\Psi_{mn}(x_1, x_2)$, viz.

$$S_w(x_1, x_2, \omega) = \sum_{m=1}^{\infty}\sum_{n=1}^{\infty} \Psi_{mn}^2(x_1, x_2)|H_{mn}(\omega)|^2\Phi_{p_{mn}}(\omega), \tag{16}$$

$$\Psi_{mn}(x_1, x_2) = 2(l_1 l_2)^{-1/2}\sin(m\pi x_1/l_1)\sin(n\pi x_2/l_2).$$

In this expression the second term

$$|H_{mn}(\omega)|^2 = 1/m_s^2[(\omega^2 - \omega_{mn}^2)^2 + (\beta\omega)^2]$$

describes the membrane frequency response, and the third term

$$\Phi_{p_{mn}}(\omega) = \int_{-\infty}^{\infty}\int_{-\infty}^{\infty} |A_m(k_1)|^2|A_n(k_2)|^2\Phi_p(k_1, k_2, \omega)\,\mathrm{d}k_1\,\mathrm{d}k_2$$

is the excitation term in which

$$|A_m(k_1)|^2 = (4/l_1)[k_m^2/(k_m^2 - k_1^2)^2][1 - (-1)^m\cos k_1 l_1], \qquad k_m = m\pi/l_1,$$

$$|A_n(k_2)|^2 = (4/l_2)[k_n^2/(k_n^2 - k_2^2)^2][1 - (-1)^n\cos k_2 l_2], \qquad k_n = n\pi/l_2,$$

are the membrane wavenumber filter shape functions for sinusoidal modes in equation (16), and $\Phi_p(k_1, k_2, \omega)$ is the wavenumber–frequency spectrum of the turbulent boundary-layer pressures. The *in vacuo* membrane natural frequencies ω_{mn} are given by

$$\omega_{mn}^2 = c^2[(m\pi/l_1)^2 + (n\pi/l_2)^2],$$

where $c = [T/m_s]^{1/2}$ is the *in vacuo* membrane wave speed.

At the structural resonances, ω_{mn}, the resonant mode response dominates and relationship (16) reduces to simplified form (here the essential condition is $l_1 \gg l_2$):

$$S_w(x_1, x_2, \omega_{mn}) = \Psi_{mn}^2(x_1, x_2)|H_{mn}(\omega_{mn})|^2\Phi_{p_{mn}}(\omega_{mn}), \tag{17}$$

$$|H_{mn}(\omega_{mn})|^2 = 1/(m_{mn}\eta_{mn}\omega_{mn}^2)^2,$$

in which m_{mn} and $\beta_{mn} = \eta_{mn}\omega_{mn}$ are the experimentally determined [4] resonant parameters of the membrane with account taken of added mass and radiation damping effects.

The final expression to be analyzed in this section is obtained from equation (17) for the case of $x_1 = l_1/2,\ x_2 = l_2/2$. For this position

$$S_w(l_1/2, l_2/2, \omega_{mn}) = \begin{cases} (4/l_1 l_2)\,|H_{mn}(\omega_{mn})|^2 \Phi_{p_{mn}}(\omega_{mn}), & \text{for both } m, n \text{ odd} \\ 0, & \text{if either } m \text{ or } n \text{ is even} \end{cases}. \quad (18)$$

This formula corresponds to formula (21) of reference [4]. It was used by the authors to obtain the predictions of displacement spectral levels, $10 \log_{10}[S_w(l_1/2, l_2/2, f_{mn})/(m^2 s)]$ (where $f_{mn} = \omega_{mn}/2\pi$; $S_w(f) = 4\pi S_w(\omega)$ [1, 4]), for the wall pressure models (10), (12), and (13). The corrected membrane response levels measured by Martin and Leehey at resonances f_{mn} in the center of the membrane (see Table 3 at $U_\infty = 40$ m/s and measured data in Figure 12 of reference [4]) were taken as the corresponding reference data. All the membrane and boundary layer parameters of reference [4] were used to determine the theoretical membrane response.

In calculating the displacement levels (18), the contributions from the acoustic, low wavenumber and convective domains of the spectrum $\Phi_p(k_1, k_2, \omega)$ in S_w were factored out and evaluated. It was done by dividing the excitation term, $\Phi_{p_{mn}}$, into three parts determined by those domains:

$$\Phi_{p_{mn}}(\omega_{mn}) \approx (\Phi_{p_{mn}}(\omega_{mn}))_{ac.} + (\Phi_{p_{mn}}(\omega_{mn}))_{low\text{–}w.n.} + (\Phi_{p_{mn}}(\omega_{mn}))_{conv.}$$

$$= \left(\int\int_{ac.} + \int\int_{low\text{–}w.n.} + \int\int_{conv.} \right) |A_m(k_1)|^2 |A_n(k_2)|^2 \Phi_p(k_1, k_2, \omega_{mn})\, \mathrm{d}k_1\, \mathrm{d}k_2,$$

and subsequent comparison of these parts with each other. For the parameters taken by Martin and Leehey the acoustic range contribution in the total membrane response was negligible in comparison with other contributions for all the models, viz.

$$(\Phi_{p_{mn}}(\omega_{mn}))_{ac.} \ll (\Phi_{p_{mn}}(\omega_{mn}))_{low\text{–}w.n.}, \qquad (\Phi_{p_{mn}}(\omega_{mn}))_{conv.},$$

$$\Phi_{p_{mn}}(\omega_{mn}) \approx (\Phi_{p_{mn}}(\omega_{mn}))_{low\text{–}w.n.} + (\Phi_{p_{mn}}(\omega_{mn}))_{conv.}.$$

Since all the wall pressure models agree at the convective wavenumber, the contribution from the convective domain to S_w was the same for all the models, viz.

$$((\Phi_{p_{mn}})_{conv.})_{F.W.} = ((\Phi_{p_{mn}})_{conv.})_{Chase} = ((\Phi_{p_{mn}})_{conv.})_{Sm.\text{–}Tk.}.$$

The most significant contribution in the response levels came from the low wavenumbers, the term $(\Phi_{p_{mn}})_{low\text{–}w.n.}$ being different for the various turbulent pressure models (because the models differ from each other in the low wavenumber domain). This is the reason for the different *relative* contribution from the convective domain in the frames of the models (10), (12) and (13). More specifically, for the Smol'yakov–Tkachenko model (13) the contribution from the convective range is of the same order of magnitude as that from the low wavenumber domain ($(\Phi_{p_{mn}})_{conv.}/(\Phi_{p_{mn}})_{low\text{–}w.n.} \times 100\% \approx 20$–$50\%$). In the frames of the Chase spectrum the convective and low wavenumber levels in S_w are very close ($(\Phi_{p_{mn}})_{conv.}/(\Phi_{p_{mn}})_{low\text{–}w.n.} \times 100\% \approx 70$–$90\%$). In the Ffowcs Williams model, the convective domain is negligible compared to the low wavenumber domain in predicting the structural response ($(\Phi_{p_{mn}})_{conv.} \ll (\Phi_{p_{mn}})_{low\text{–}w.n.}$).

The predicted and experimental levels of the membrane displacement are shown in Figure 3. Since the low wavenumber range dominates each model's overall prediction, the theoretical response levels for the different wavenumber–frequency models thus mainly reflect their low wavenumber behaviour (although the convective ridge contribution is also reflected in the responses to the extent noted above). This is the reason for the different

predictions of the Chase, Ffowcs Williams, and Smol'yakov–Tkachenko models. By comparison of the experimental and theoretical responses, one can see that the Chase model prediction has the best agreement with the experimental data of reference [4]. The Smol'yakov–Tkachenko spectrum predicts the structural response not so well as the Chase spectrum. However, the Smol'yakov–Tkachenko model prediction is significantly better than that for the Ffowcs Williams model, reflecting its reduced low wavenumber levels in $\Phi_p(k_1, k_2, \omega)$.

Thus, in this section the effect of differing choices of the wavenumber–frequency spectrum model on the response of a boundary-layer driven membrane has been considered, and the corresponding predictions of the response have been compared with the experimental data of Martin and Leehey. The results obtained show that, for the ranges of parameters considered, the Chase and Smol'yakov–Tkachenko models give the best predictions of turbulence induced fields. We conclude, therefore, that these models are suitable for predictions of turbulence induced fields for these or close ranges of flow and structural parameters. As to the Ffowcs Williams model, its significant overprediction of the structural response can be probably due to the incorrect choice of the functions and constants in equation (11) to be determined experimentally. Unfortunately, it was not possible to carry out the desired experiments for several reasons and therefore the choice of expressions and values for the mentioned functions and constants have been restricted to those available in the scientific literature [11]. This reduced expression (11) to the expression (12) used in this study.

Finally, it should be noted that the conclusions made by the authors are restricted to the case considered here, and, consequently, further research is likely to be necessary for cases of particular interest.

4. THE ROLE OF THE DIFFERENT WALL PRESSURE COMPONENTS

As noted in the Introduction, the Corcos model is based on the assumption that the energy-containing convective domain can be neglected in estimating the fields generated by low Mach number turbulence. However, this domain can be an important contributor when the other, more adequate, models for the wavenumber-frequency spectrum, Φ_p, are used to describe the random surface pressure field, p_t. This prediction has been just confirmed for the case of a turbulent-boundary-layer-excited membrane, and the corresponding quantitative estimates of the various wall pressure component contributions have been obtained for the pressure fluctuation models considered in this study. It is

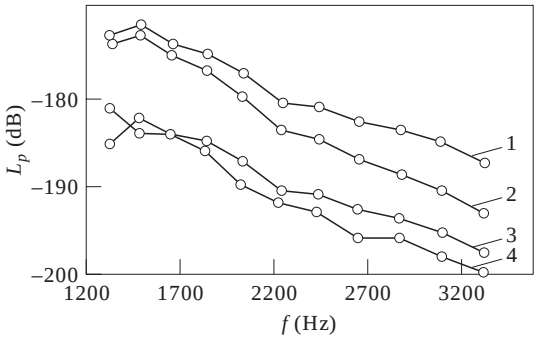

Figure 3. Predicted and experimental spectral levels of membrane displacement, $L_p = 10 \lg [S_w(l_1/2, l_2/2, f)/(\mathrm{m^2 s})]$, $f = \omega/2\pi$. Membrane responses for 1, Ffowcs Williams model; 2, Smol'yakov–Tkachenko model; 3, Chase model; 4, experimental levels measured by Martin and Leehey.

obvious that for each plane configuration of streamlined elastic structure, and boundary and flow conditions taken, the accurate quantitative estimates of those contributions in the fields generated will be different. However, the conclusions about the role of the components must be qualitatively identical (namely, the components are important or not for the conditions of interest). It is reasonable, therefore, to illustrate qualitatively, through simple problems, in basic physical terms, the role of the acoustic, low wavenumber, and convective components in the fields generated by low Mach number turbulence. In connection with this in this section simple problems of the generation of sound by a one-dimensional structure driven separately by these components are treated, and the corresponding radiated acoustic powers for the cases of two characteristic combinations of basic parameters which determine the efficiency of sound radiation by the components are compared. By means of this comparison, conclusions about the importance of the components can be made.

4.1. THE GENERATION OF SOUND BY THREE TYPES OF MODES OF ELASTIC STRIP

The efficiency of sound radiation by a turbulent wall pressure component $P(\alpha, \omega) \sin \alpha x \, e^{-i\omega t}$ due to turbulence–elastic structure interaction is mainly determined by three basic factors. These are the amplitude P (or power $\sim P^2$), the spatial wavenumber α (or spatial variability of the component), and the location of the driven frequency ω with respect to the natural frequency of the elastic structure. The acoustic, $P_1(\alpha_1, \omega) \sin \alpha_1 x \, e^{-i\omega t}$, low wavenumber, $P_2(\alpha_2, \omega) \sin \alpha_2 x \, e^{-i\omega t}$, and convective $P_3(\alpha_3, \omega) \sin \alpha_3 x \, e^{-i\omega t}$, wall pressure components are characterized by significantly different amplitudes, and significantly different wavenumbers. This reflects the inner nature of the turbulence, while the driven/natural frequencies ratio characterizes the coupling between the resonant properties of the streamlined elastic element and the properties of the turbulent flow. It is interesting to know how the efficiency of sound radiation by the components depends on their pure turbulent nature, and how the efficiency is then influenced by the coupling mechanism. In connection with this one considers the corresponding two model problems which illustrate these dependencies. The first of them shows the influence of the powers and spatial variabilities of the turbulent wall pressure components on the acoustic power produced by the turbulence excited elastic structure. The frequency dependence is omitted here. Since the structural response is weakly dependent on frequency away from structural resonances, here the question is in fact about the non-resonant excitation of elastic body by the various wall pressure components.

Thus, the following acoustic problem is under consideration. The strip (one-dimensional plate) of width l is simply supported in an infinite rigid baffle. Let the normal velocity distribution $V(\alpha) \sin \alpha x \, e^{-i\omega t}$ on the surface (which has been induced by the wall pressure p_t) strongly corresponds to the strip normal mode $\Psi_m(x) = \sin k_m x$, viz., $V(\alpha) \sin \alpha x = V(\alpha) \sin k_m x$, where $k_m = m\pi/l$ is the structural wavenumber. The acoustic power Π generated separately by the three types of velocity distributions

$$V_1 \sin \alpha_1 x = V_1 \sin k_m x, \qquad \alpha_1 = k_m = m\pi/l < k_0, \qquad V_2 \sin \alpha_2 x = V_2 \sin k_n x,$$

$$k_0 < \alpha_2 = k_n = n\pi/l \ll k_c, \qquad V_3 \sin \alpha_3 x = V_3 \sin k_s x, \qquad \alpha_3 = k_s = s\pi/l \approx k_c, \quad (19)$$

is to be determined. The amplitudes and wavenumbers (V_1, α_1), (V_2, α_2), and (V_3, α_3) correspond to the acoustic, low-wavenumber and convective domains in the wavenumber–frequency spectrum Φ_p, respectively (see Figure 4; dashed domains are the radiating ones [18]).

In mathematical terms, one needs to find the power Π of the acoustic field $p_0(x, z) \, e^{-i\omega t}$ satisfying the two-dimensional, in the (x, z) plane, Helmholtz equation

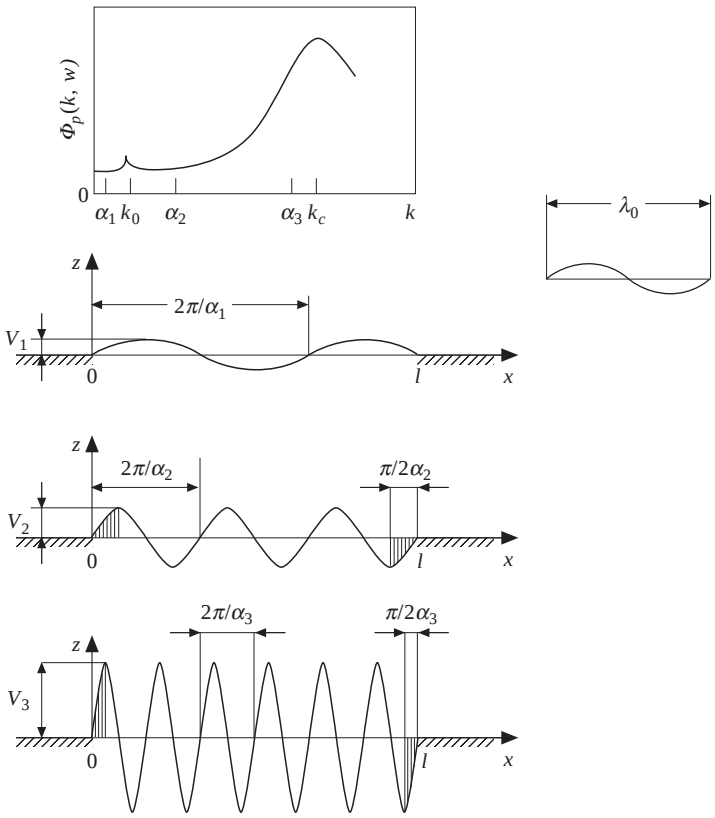

Figure 4. Surface-radiating acoustic modes, $V_1 \sin \alpha_1 x$, and corner-radiating low wavenumber, $V_2 \sin \alpha_2 x$, and convective, $V_3 \sin \alpha_3 x$, modes of a simply supported strip. The modes are determined by the acoustic ($\alpha_1 < k_0$), low wavenumber ($k_0 < \alpha_2 \ll k_c$), and convective ($\alpha_3 \approx k_c$) domains of the wavenumber–frequency spectrum $\Phi_p(k, \omega)$ of the turbulent wall pressure with $\omega = const$. The radiating domains of the corner-radiating modes are dashed.

$$\nabla^2_{(x,z)} p_0 + k_0^2 p_0 = 0, z > 0, \tag{20}$$

with the boundary conditions:

$$\partial p_0 / \partial z|_{z=0} = \mathrm{i}\rho_0 \omega v, \quad 0 < x < l, \qquad v = 0, \quad x \leqslant 0, \quad x \geqslant l, \tag{21}$$

in which v is one of the three expressions in equations (19).

The solution to the problem (20), (21) is obtained by the use of the spatial Fourier transform

$$g(k) = \frac{1}{(2\pi)} \int_{-\infty}^{\infty} g(x)\, \mathrm{e}^{-\mathrm{i}kx}\, \mathrm{d}x,$$

and taking the Fourier transformed acoustic pressure to be of the direct wave form

$$p_0(k, z) = A(k)\, \mathrm{e}^{\mathrm{i}(k_0^2 - k^2)^{1/2} z},$$

where the unknown factor $A(k)$ is found from the Fourier transformed boundary

conditions (21). Then the power Π, defined as the real part of the integral

$$\int_0^l p_0^*(x, z = 0)v(x)\,\mathrm{d}x$$

(here the asterisk denotes a complex conjugate), has the form

$$\Pi_j = l\rho_0 c_0 \sigma_j V_j^2/2, \quad j = 1, 2, 3, \tag{22}$$

where σ_j is the radiation efficiency coefficient of the jth mode in equations (19),

$$\sigma_j = \frac{4}{l}\frac{1}{2\pi}\int_0^{k_0} \frac{|A_j(k)|^2}{(1 - k^2/k_0^2)^{1/2}}\,\mathrm{d}k,$$

and $|A_j(k)|^2$ is the modal shape function given by the expression:

$$|A_j(k)|^2 = \frac{2\alpha_j^2}{(\alpha_j^2 - k^2)^2}\,[1 - (-1)^r \cos{(kl)}]$$

(here $r = m$ for $j = 1$, $r = n$ for $j = 2$, and $r = s$ for $j = 3$).

The acoustic powers (22) are mainly determined by the amplitudes V_j and the radiation efficiency coefficients σ_j of the modes (19). Of these modes, the acoustic ones are characterized by very small amplitudes compared with the other modes, viz., $V_1 < V_2 \ll V_3$, and very low spatial variabilities (see Figure 4), viz., high radiation efficiencies, $\sigma_1 = \sigma_m \approx 1$ (these are surface-radiating high efficiency modes [18]). The low-wavenumber modes have small amplitudes and relatively low wavenumbers, viz., relatively low radiation efficiencies, $\sigma_2 = \sigma_n < 1$ (these are corner-radiating low-efficiency modes with the dimensions of the radiative domains equal to one-fifth of the structural wavelength $2\pi/\alpha_2$ [18]). The amplitudes and spatial variabilities of the convective modes are, in contrast to those of the acoustic and low-wavenumber modes, very high, viz., $V_3/V_1 > V_3/V_2 \gg 1$, $\sigma_3 = \sigma_s \ll 1$. These are also corner-radiating low-efficiency modes [18], but the dimensions of their radiative domains are much smaller than those of the low-wavenumber modes, viz., $\pi/2\alpha_3 \ll \pi/2\alpha_2$. As a result, $\sigma_3 \ll \sigma_2$. To understand which of the modes (19) are the most efficient radiators of sound, one considers the difference between the spectral levels of the acoustic powers (22),

$$\Delta_i = 10 \lg{(\Pi_i/\Pi_3)} = 10 \lg{(\sigma_i/\sigma_3)} + 10 \lg{(V_i^2/V_3^2)}, \quad i = 1, 2, \tag{23}$$

produced by the acoustic ($i = j = 1$) and convective ($j = 3$) modes, and low-wavenumber ($i = j = 2$) and convective ($j = 3$) modes. One can see that the parameter Δ_i is the sum of two terms. The first is the ratio of the radiation efficiency coefficients of the modes (19) and the second is the ratio of the squares of the modal velocity amplitudes which is in fact the ratio of the modal powers. Since the power of vibrations is determined by the input power, one can relate the ratio of the excitation force powers to the ratio of the corresponding mode powers. Since the modes (19) correspond to three different domains of the wavenumber–frequency spectrum Φ_p, the second term in equation (23) can be replaced by the difference in the spectral levels of the corresponding pressure fluctuation components, $10 \lg P_i^2/P_3^2$, viz.,

$$\Delta_i \approx 10 \lg{(\sigma_i/\sigma_3)} + 10 \lg{(P_i^2/P_3^2)}. \tag{24}$$

As a result, the differences between the components will be taken into account in the frames of the existing wall pressure models.

TABLE 1

Approximate component spectral level differences for the different models

Model	Difference between the component spectral levels (dB)	
	Convective and low wavenumber	Convective and acoustic
Corcos	16–19	20
Ffowcs Williams	27–42	45–50
Smol'yakov–Tkachenko	38–45	50–55
Chase	40–60	65–70

An approximate difference between the component spectral levels for the various models (according to the works [10, 11]) is given in Table 1. The results of the evaluation of Δ_i, obtained for the cases $l = \lambda_0$ and $l = 2\lambda_0$, are presented in Table 2. In both cases the first mode was chosen as acoustic ($i = j = 1, m = 1$) and the sixth ($l = \lambda_0, n = 6$) and the twelfth ($l = 2\lambda_0, n = 12$) were chosen as low-wavenumber modes ($i = j = 2$). The convective Mach number $M_c = U_c/c_0$ was taken to be equal to 10^{-2}, and the following approximate expressions for σ_j have been used [16]:

$$\sigma_1 = \sigma_m = 1, \qquad \sigma_2 = \sigma_n = (2k_0/k_n^2 l)[1 - (-1)^n \mathrm{J}_0(k_0 l)], \qquad k_n > 2k_0,$$
$$\sigma_3 = \sigma_s = (2/k_0 l)M_c^2[1 - (-1)^s \mathrm{J}_0(k_0 l)], \qquad k_s \approx k_c \gg 2k_0, \tag{25}$$

where J_0 is the cylindrical Bessel function of the first kind and zero order.

The last formula is interesting in that it directly determines the radiation efficiency coefficients of the modes for which the structural wavenumber is close to the convective wavenumber, in terms of both the wave dimension, $k_0 l$, of the vibrating elastic element and the properties of the turbulent flow (via the inclusion of the convective Mach number, M_c). One can see that, on the one hand, the smaller $k_0 l$ the more efficient are the modes for which $k_s \approx k_c$ and *vice versa*. On the other hand, the modal radiation efficiency increases as M_c^2 as the turbulent convective velocity increases.

The estimates obtained (it should be noted that the estimates would be approximately the same for the other modes satisfying equations (19)) show that in the framework of the Corcos model the acoustic and low wavenumber modes exceed the convective ones in their ability to generate the acoustic far field. However, this result is refuted by the estimates obtained for three other models. In their frameworks the sound power radiated by the convective modes is much higher than that radiated by the other types of modes (for the Ffowcs Williams model the acoustic and convective modes are similar radiators of sound). In terms of the basic physical parameters considered in this paragraph, this means that in formulas (23) and (24) the second term dominates. In other words, although the effective

TABLE 2

Results of the evaluation of Δ_i for the different models

l	Δ_i	Model			
		Corcos	Ffowcs Williams	Smol'yakov–Tkachenko	Chase
λ_0	Δ_1	26	0	−7	−21
	Δ_2	11	−10	−15	−25
$2\lambda_0$	Δ_1	29	3	−4	−18
	Δ_2	11	−10	−15	−25

radiating surface of the convective modes is much smaller than that of the other modes, viz.:

$$10 \lg \sigma_i/\sigma_3 \gg 1, \quad i = 1, 2,$$

their large amplitudes V_3 permit them to dominate the other modes in the acoustic power radiated away from structural resonances.

Thus, the results obtained in this paragraph allow us to conclude that according to the Chase, Ffowcs Williams and Smol'yakov–Tkachenko models (which more adequately describe turbulent excitation than the Corcos model) the convective wall pressure components generate noise more effectively away from structural resonances than the acoustic and low-wavenumber components. The efficiency of sound generation by the components is determined by their amplitudes (powers) rather than spatial variabilities. Among other consequences, this result permits one to talk about the dominant role of the process of the short wavelength convective component energy transformation at surface inhomogeneities. This conclusion is in a good agreement with Crighton's results [13].

4.2. THE GENERATION OF SOUND BY STRIP EXCITED BY THREE TYPES OF THE WALL PRESSURE COMPONENTS

In this section the influence of coupling between the resonant properties of the streamlined elastic body and the properties of the turbulent flow on the estimates obtained in section 4.1. is studied. For this purpose the plane problem of the sound radiation by the same elastic strip excited separately by the acoustic, low-wavenumber, and convective wall pressure components is considered. The spatial variabilities of the components strongly correspond to those of the strip normal modes, viz.,

$$P_1 \sin \alpha_1 x = P_1 \sin k_m x, \qquad \alpha_1 = k_m < k_0, \qquad P_2 \sin \alpha_2 x = P_2 \sin k_n x,$$
$$k_0 < \alpha_2 = k_n \ll k_c, \qquad P_3 \sin \alpha_3 x = P_3 \sin k_s x, \qquad \alpha_3 = k_s \approx k_c. \tag{26}$$

The acoustic power Π radiated by the strip is unknown as before.

In this formulation, the normal velocity of the strip vibration, $v(x)\, e^{-i\omega t}$, and the acoustic pressure, $p_0(x, z)\, e^{-i\omega t}$, satisfy the coupled equations of motion,

$$D_s d^4v/dx^4 - m_s\omega^2 v = i\omega(p_t + p_0|_{z=0}), \qquad 0 < x < l, \tag{27}$$

and acoustics,

$$\nabla^2_{(x,z)} p_0 + k_0^2 p_0 = 0, \quad z > 0, \tag{28}$$

with boundary conditions

$$v|_{x=0,l} = 0, \qquad d^2v/dx^2|_{x=0,l} = 0, \qquad \partial p_0/\partial z|_{z=0} = i\rho_0\omega v$$
$$0 < x < l, \quad v = 0, \qquad x \leqslant 0, \qquad x \geqslant l, \tag{29}$$

in which p_t is taken to be one of the three expressions in equations (26).

The use of the spatial Fourier transform defined in section 4.1. and performing a modal analysis

$$v(x) = \sum_{m=1}^{\infty} V_m \Psi_m(x)$$

allow one to obtain the solution of the problem (27)–(29). Leaving aside all the details, one can write the final expression for the acoustic power radiated as

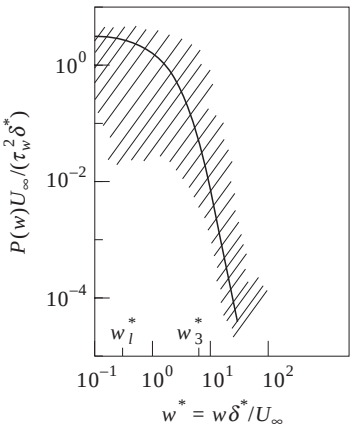

Figure 5. Wall pressure power spectrum $P(\omega)$. The region of the experimental data available in periodicals is dashed.

$$\Pi_j = l\rho_0 c_0 \sigma_j |V_j|^2/2, \qquad j = 1, 2, 3,$$
$$V_j = \mathrm{i}\omega P_j/(m_s[\omega_j^2 - \omega^2(1 + m_j(\omega)/m_s)] - [\mathrm{i}\omega\rho_0 c_0 \sigma_j(\omega)]). \tag{30}$$

Here $\omega_j = (D_s/m_s)^{1/2}k_j^2$, and

$$m_j(\omega) = \frac{\rho_0 c_0}{\omega}\frac{4}{l}\frac{1}{2\pi}\int_{k_0}^{\infty}\frac{|A_j(k)|^2}{(k^2/k_0^2 - 1)^{1/2}}\,\mathrm{d}k$$

are the natural frequency and the specific added mass of the strip's jth mode, respectively. Formula (30) is physically more substantial than formula (22). The modal velocity amplitude V_j in equation (30) is determined not only by the corresponding wall pressure amplitude P_j but also by the resonant and radiation damping effects. Each of these parameters influences the power value Π_j in a certain way.

Parameters Δ_i characterizing the difference in the power radiated levels can be rewritten in the form

$$\Delta_i = 10\lg(\sigma_i/\sigma_3) + 10\lg(P_i^2/P_3^2) + \delta_i,$$
$$\delta_i = 10\lg\frac{[\omega_3^2/\omega^2 - (1 + m_3(\omega)/m_s)]^2 + [\rho_0 c_0 \sigma_3(\omega)/m_s\omega]^2}{[\omega_i^2/\omega^2 - (1 + m_i(\omega)/m_s)]^2 + [\rho_0 c_0 \sigma_i(\omega)/m_s\omega]^2}, \qquad i = 1, 2. \tag{31}$$

One can see that there is a similarity in the first two terms of equation (31) and equations (23), (24). The difference between equation (31) and equations (23), (24) is in the third term δ_i in which the resonant properties of the modes (the coupling effects of interest) are contained. To determine its value it is necessary to take physically reasonable frequencies (although theoretically they can be arbitrary). To do this one can look at the wall pressure power spectrum $P(\omega)$ shown in Figure 5. The pressure fluctuations have a small part of the energy at high frequencies and the elastic structures excited by those frequency components generate very low noise levels. The levels are not very different from the instrumentation noise levels. The main part of the turbulent energy is concentrated at low frequencies. That is why one should use relatively low frequencies to estimate δ_i. Furthermore, the mechanical and geometrical characteristics of the elastic element have to be chosen in such a way that, for the frequency scales U_∞/δ^* in the turbulent boundary layer flow, the natural frequencies of the lower modes belong to the given frequency interval. The acoustic and low-wavenumber modes can be considered to be the lower

modes. This permits one to talk about the corresponding resonances $\omega = \omega_i$ in equation (31). The convective mode resonances $\omega = \omega_3$ will not appear in equation (31), because their frequencies are very high ($\omega_3 \gg \omega_2 > \omega_1$) and belong to the high frequency limit in $P(\omega)$.

The estimates for the third term, δ_i, in equation (31), obtained for the case of resonances of the acoustic and low wavenumber modes, $\omega = \omega_i$, are given in Table 3. Non-resonant excitation has effectively been considered in section 4.1. In the calculations, the same mode numbers, etc., as in Table 2 and the following parameter values have been used: $l = 1$ m, $h = 0{\cdot}02$ m, $\rho_s = 8000$ kg/m^3 (width, thickness and mass density of the strip, respectively), $c_p = 4500$ m/s (bending wave speed in the strip material), $\rho_s/\rho_0 = 8$, $c_p/c_0 = 3$. The added masses m_j have been represented by the expressions [16]

$$m_1 = m_m = 0, \qquad m_2 = m_n = \rho_0/k_n, \qquad k_n > 2k_0, \qquad m_3 = m_s = \rho_0/k_c, \qquad k_s \approx k_c \gg 2k_0.$$

Adding the data from Table 3 to the corresponding data from Table 2 (as it follows from the comments on formulas (23), (24), and (31), the estimates in Table 2 are in fact the sum of the first two terms in formula (31)) one obtains the positive values of the parameters Δ_i for all the pressure fluctuation field models. This result shows that for all the models the acoustic and low-wavenumber wall pressure components at the resonances $\omega = \omega_i$ of the corresponding structural normal modes generate sound more effectively than the convective components. However, the role of the convective components will gradually increase as the driving frequency moves away from the natural frequencies ω_i (coupling effects become less important, viz., δ_i decreases) and, starting from some frequency ω, the sound radiated by them will dominate in the total sound field.

Thus, these results correct the conclusions of the previous section near the structural resonances $\omega = \omega_i$. In this domain the acoustic and low wavenumber wall pressure components generate noise of higher intensity than the convective components. Besides, since near these resonances the coupling effects dominate, even such a large difference in the spectrum levels of the wall pressure components (which is in the models of references [8–10]; see Table 1) cannot essentially influence the estimates.

5. SOUND FROM TURBULENCE EXCITED PANEL

In this section a turbulent-boundary-layer-driven plate is considered and the predictions of radiated sound for the turbulent wall pressure models of Corcos, Chase, Ffowcs Williams, and Smol'yakov–Tkachenko are analyzed.

5.1. STATEMENT OF THE PROBLEM

The following acoustic problem is under discussion. A simply supported thin rectangular elastic plate of length l_1 in the direction of mean flow x_1 and of width l_2 is inserted in a flat infinite rigid baffle. The plate vibrations are excited by a turbulent wall pressure fluctuations $p_t(x_1, x_2, t)$ on the upper surface of the plate. The random field $p_t(x_1, x_2, t)$

TABLE 3

Estimates of δ_i in equation (31)

δ_i	$l = \lambda_0$	$l = 2\lambda_0$
δ_1	153	177
δ_2	131	137

is considered to be statistically stationary in time and homogeneous in space. The acoustic power radiated by the plate to the side away from the flow ($x_3 > 0$) is unknown.

In formulating a problem on the excitation of vibrations by a turbulent boundary layer, one should pay attention to the following assumption. In real situations, the characteristics of the turbulent boundary layer change along the surface of the streamlined structure. In connection with this, we assume that the developed turbulent boundary layer measured at different sections of the flow will differ only in the intensity of pressure fluctuations (power spectrum), while the spatial distribution of the fluctuation field remains invariant.

If the influence of the panel vibration on the boundary layer, as well as the interaction between boundary layer and acoustic pressures are neglected, then the equation of the plate motion written for the plate normal velocity $v(x_1, x_2, t)$ is [1, 2, 16, 19–23]:

$$m_s \partial^2 v/\partial t^2 + \beta \partial v/\partial t + D_s \nabla^4 v = -(\partial/\partial t)(p_t + p_0|_{x_3 = 0}), \tag{32}$$

with corresponding boundary conditions

$$v|_{x_1 = 0, l_1} = v|_{x_2 = 0, l_2} = 0, \qquad \partial^2 v/\partial x_1^2|_{x_1 = 0, l_1} = \partial^2 v/\partial x_2^2|_{x_2 = 0, l_2} = 0, \tag{33}$$

where $p_0(x_1, x_2, x_3, t)$ is the acoustic pressure generated by the motion of the panel, D_s the plate bending stiffness, m_s its mass per unit area, and β is a coefficient introduced to account for mechanical damping of the panel through a linear dependence on velocity. D_s is related to the plate Young's modulus E, thickness h, and Poisson's ratio ν, by $D_s = Eh^3/12(1 - \nu^2)$.

In the classical model of an inviscid compressible fluid, p_0 satisfies the wave equation, with sound speed c_0

$$\nabla^2 p_0 - (1/c_0^2)\partial^2 p_0/\partial t^2 = 0, \qquad x_3 > 0, \tag{34}$$

and the system of equations (32)–(34) is completed by the condition linking p_0 and v at the plate surface,

$$\partial p_0/\partial x_3|_{x_3 = 0} = -\rho_0 \partial v/\partial t, \tag{35}$$

where ρ_0 is the density of the acoustic medium, and by the condition on the rigid baffle,

$$v = 0. \tag{36}$$

5.2. ANALYSIS

The solution of the problem (32)–(36) is obtained by taking the Fourier transform, defined here as

$$g(k_1, k_2, x_3, \omega) = \frac{1}{(2\pi)^3} \int_{-\infty}^{\infty} \int_{-\infty}^{\infty} \int_{-\infty}^{\infty} g(x_1, x_2, x_3, t)\, \mathrm{e}^{-\mathrm{i}(k_1 x_1 + k_2 x_2 - \omega t)}\, \mathrm{d}x_1\, \mathrm{d}x_2\, \mathrm{d}t, \tag{37}$$

and performing a modal analysis. The *in vacuo* modes $\Psi_{mn}(x_1, x_2)$ of the simply supported panel satisfy the equation

$$D_s \nabla^4 \Psi_{mn} - \omega_{mn}^2 m_s \Psi_{mn} = 0 \tag{38}$$

and the boundary conditions (33) and are given by the expression

$$\Psi_{mn}(x_1, x_2) = \sin k_m x_1 \sin k_n x_2, \tag{39}$$

with modal wavenumbers $k_m = m\pi/l_1$, $k_n = n\pi/l_2$ and *in vacuo* natural frequencies of the plate:

$$\omega_{mn} = (D_s/m_s)^{1/2}(k_m^2 + k_n^2) = (D_s/m_s)^{1/2} k_{mn}^2. \tag{40}$$

The modal equations are found by writing the velocity in equation (32) as an infinite sum of individual mode components,

$$v(x_1, x_2, \omega) = \frac{1}{2\pi}\int_{-\infty}^{\infty} v(x_1, x_2, t)\, e^{i\omega t}\, dt = \sum_{m=1}^{\infty}\sum_{n=1}^{\infty} V_{mn}(\omega)\Psi_{mn}(x_1, x_2) \tag{41}$$

and using the orthogonality properties of the normal modes. This process yields

$$m_s[(\omega_{mn}^2 - \omega^2) - i\omega^2\eta_s]V_{mn} = i\omega p_{t_{mn}}(\omega) + i\omega p_{0_{mn}}(\omega), \tag{42}$$

where η_s is a loss factor given by $\eta_s\omega = \beta/m_s$, and $p_{t_{mn}}$ and $p_{0_{mn}}$ are of similar form and defined by

$$p_{t_{mn}}(\omega) = (4/l_1 l_2)\int_0^{l_1}\int_0^{l_2} p_t(x_1, x_2, \omega)\Psi_{mn}(x_1, x_2)\, dx_1\, dx_2,$$

$$p_{0_{mn}}(\omega) = (4/l_1 l_2)\int_0^{l_1}\int_0^{l_2} p_0(x_1, x_2, 0, \omega)\Psi_{mn}(x_1, x_2)\, dx_1\, dx_2, \tag{43}$$

The acoustic pressure can be found from equations (34)–(37), in the form

$$p_0(x_1, x_2, x_3, \omega) = \frac{\rho_0 c_0}{(2\pi)^2}\sum_{m=1}^{\infty}\sum_{n=1}^{\infty} V_{mn}(\omega)Q_{mn}(x_1, x_2, x_3, \omega), \tag{44}$$

in which

$$Q_{mn}(x_1, x_2, x_3, \omega) = \int_{-\infty}^{\infty}\int_{-\infty}^{\infty} \frac{A_m(k_1)A_n(k_2)\, e^{i(k_1 x_1 + k_2 x_2 + (k_0^2 - k_1^2 - k_2^2)^{1/2} x_3)}}{(1 - (k_1^2 + k_2^2)/k_0^2)^{1/2}}\, dk_1\, dk_2$$

and $(1/2\pi)^2 A_m(k_1)A_n(k_2)$ are the spatial Fourier transforms of the normal modes Ψ_{mn} in equation (39).

With the expression (44), the acoustic pressure modal components $p_{0_{mn}}(\omega)$ in equation (43) may now be related to the modal velocity amplitudes by

$$p_{0_{mn}}(\omega) = \sum_r\sum_s Z_{mnrs}(\omega)V_{rs}(\omega), \tag{45}$$

where the modal impedances

$$Z_{mnrs}(\omega) = \frac{\rho_0 c_0}{|\Psi_{mn}|^2}\frac{1}{(2\pi)^2}\int_{-\infty}^{\infty}\int_{-\infty}^{\infty} \frac{A_m^*(k_1)A_r(k_1)A_n^*(k_2)A_s(k_2)}{(1 - (k_1^2 + k_2^2)/k_0^2)^{1/2}}\, dk_1\, dk_2$$

(here the asterisk denotes a complex conjugate) describe the contribution of the (r, s) modal velocity to the (m, n) modal acoustic pressure, and Z_{mnrs} are zero unless $(m + r)$ and $(n + s)$ are both even [16, 20, 21]. On substituting expression (45) into equation (42), the

acoustic field becomes coupled to the modal response equations:

$$m_s[(\omega_{mn}^2 - \omega^2) - \mathrm{i}\omega^2\eta_s - \mathrm{i}\omega Z_{mnmn}/m_s]V_{mn} - \mathrm{i}\omega\Bigg[\sum_{s\neq n} Z_{mnms}V_{ms} + \sum_{r\neq m} Z_{mnrn}V_{rn} + \sum_{r\neq m}\sum_{s\neq n} Z_{mnrs}V_{rs}\Bigg] = \mathrm{i}\omega p_{t_{mn}}(\omega). \quad (46)$$

An exact solution of equation (46) can be found in references [16, 20, 21]. In this work, however, the coupling effect is ignored, and therefore one is restricted to the consideration of the so-called diagonal solution

$$V_{mn}(\omega) = [\mathrm{i}\omega/a_{mn}(\omega)]p_{t_{mn}}(\omega). \quad (47)$$

The neglect of the coupling effect is justified by the following reasons. Firstly, in most practical circumstances [1, 16, 20–24] this effect is negligible. Secondly, in this section the effect of the choice of the turbulent wall pressure model on the predictions of sound radiated is studied. In this case the coupling effect is of secondary importance (because the inclusion of the coupling results in only a few percent change of the diagonal solution, while the differences between the models cause differences of at least 10 dB (ten times!) in the sound power predictions), and this results mainly in a significant increase of calculations rather than exposition of the effect studied: that of the choice of models.

In formula (47) the denominator is given by the expression

$$a_{mn}(\omega) = m_s\left[\omega_{mn}^2 - \left(1 + \frac{m_{mn}(\omega)}{m_s}\right)\omega^2 - \mathrm{i}\omega^2\left(\eta_s + \frac{\rho_0 c_0 \sigma_{mn}(\omega)}{m_s\omega}\right)\right] \quad (48)$$

and $\sigma_{mn}(\omega)$ and $m_{mn}(\omega)$ are the specific radiation efficiency and specific added mass of the (m, n)th mode, respectively. These terms are defined as the real and imaginary parts of the specific radiation impedance, $Z_{mnmn}(\omega)$, of mode (m, n), respectively:

$$Z_{mnmn}(\omega) = \rho_0 c_0 \sigma_{mn}(\omega) - \mathrm{i}\omega m_{mn}(\omega) = \frac{4}{l_1 l_2}\frac{\rho_0 c_0}{\pi^2}\int_0^\infty\int_0^\infty \frac{|A_m(k_1)|^2|A_n(k_2)|^2}{(1 - (k_1^2 + k_2^2)/k_0^2)^{1/2}}\,\mathrm{d}k_1\,\mathrm{d}k_2 \quad (49)$$

with the shape functions

$$|A_m(k_1)|^2 = A_m(k_1)A_m^*(k_1) = [2k_m^2/(k_m^2 - k_1^2)^2][1 - (-1)^m\cos(k_1 l_1)],$$
$$|A_n(k_2)|^2 = A_n(k_2)A_n^*(k_2) = [2k_n^2/(k_n^2 - k_2^2)^2][1 - (-1)^n\cos(k_2 l_2)]. \quad (50)$$

An expression for the average sound power radiated to one side of the panel can thus be found. The spectral density of the power radiated, $\Pi(\omega)$, is just the integral of the acoustic pressure velocity product over the area of the panel [1]. Thus,

$$\Pi(\omega)\delta(\omega - \omega') = \int_0^{l_1}\int_0^{l_2}\langle p_0^*(x_1, x_2, 0, \omega)v(x_1, x_2, \omega')\rangle\,\mathrm{d}x_1\,\mathrm{d}x_2, \quad (51)$$

where it is implicit that the acoustic radiation is described by the real part of the integral and the brackets denote an ensemble average and δ is the Dirac delta function. When values of the panel velocity (41), (47) and acoustic pressure (44) are substituted into

equation (51), and the integration is performed, the power spectral density becomes

$$\Pi(\omega) = \sum_{m=1}^{\infty}\sum_{n=1}^{\infty} \Pi_{mn}(\omega) = \frac{l_1 l_2}{4}\rho_0 c_0 \omega^2 \sum_{m=1}^{\infty}\sum_{n=1}^{\infty} \frac{\sigma_{mn}(\omega)}{|a_{mn}(\omega)|^2}\Phi_{p_{mn}}(\omega), \tag{52}$$

where $\Phi_{p_{mn}}(\omega)$ is the modal excitation term, defined in terms of the wavenumber-frequency spectrum of the turbulent boundary layer pressure $\Phi_p(k_1, k_2, \omega)$, as

$$\Phi_{p_{mn}}(\omega) = \frac{4}{(l_1 l_2)^2}\int_{-\infty}^{\infty}\int_{-\infty}^{\infty} |A_m(k_1)|^2 |A_n(k_2)|^2 \Phi_p(k_1, k_2, \omega)\,\mathrm{d}k_1\,\mathrm{d}k_2. \tag{53}$$

Thus the total acoustic power radiated by the plate, $\Pi(\omega)$, is a sum of individual mode contributions, $\Pi_{mn}(\omega)$, the powers $\Pi_{mn}(\omega)$ being determined by the three factors in the behaviour of the problem. Firstly, this is the degree of excitation of the (m, n)th mode which is represented by the modal excitation term $\Phi_{p_{mn}}(\omega)$. This term depends on two factors, namely the amplitudes of the wall pressure components and their spatial correlations with the normal mode $\Psi_{mn}(x_1, x_2)$. Secondly, this is the modal radiation efficiency coefficient $\sigma_{mn}(\omega)$. Its magnitude depends on the degree of the spatial variability of displacements in the plane of the plate [1, 16, 18–24]. The other conditions being equal, the higher the spatial variability of the given normal mode $\Psi_{mn}(x_1, x_2)$ (viz., the more nodal lines it has) the lower the emitted energy. Finally, the modal acoustic power $\Pi_{mn}(\omega)$ is influenced by the structural response term $a_{mn}(\omega)$ in which the resonant effects are reflected. $a_{mn}(\omega)$ is seen from equation (48) to have a minimum value when the driving frequency ω coincides with the modal resonance frequency $\omega_{mn}/(1 + m_{mn}/m_s)^{1/2}$ estimated with the inclusion of the added mass m_{mn}, and the mode's response is controlled by the imaginary part of $a_{mn}(\omega)$, which arises from the structural damping term η_s and the modal radiation damping term $\rho_0 c_0 \sigma_{mn}/m_s\omega$.

Since the effect of the turbulent boundary layer on the radiated acoustic power $\Pi(\omega)$ is essentially reflected in the excitation term (53) (via the wavenumber-frequency spectrum $\Phi_p(k_1, k_2, \omega)$), the expected differences in the predictions of the power for the different wall pressure models will thus be associated with the different magnitudes of $\Phi_{p_{mn}}(\omega)$. These differences are mainly due to the different contributions of the subconvective wall pressure components as assumed in the models (the convective component contribution is the same for all the models, but their *relative* contributions are significantly different; see, for example, the considerations after formula (18)). The analysis of expressions (52) and (53) shows that in the solution (52) the long wavelength subconvective ($k_1 \ll k_c$) and short wavelength convective ($k_1 \approx k_c$) components manifest themselves in the following way [16]. First of all, they excite the modes which are spatially correlated with them (the long wavelength, $k_m \ll k_c$, and convective, $k_m \approx k_c$, modes, respectively). In addition, the long wavelength components excite also the convective modes, and the convective components, in turn, excite the long wavelength modes. Both types of modes contribute to the sound radiated by the plate. However, the weights of those contributions are different. The whole situation is determined by the driving frequency, its position relative to the plate coincidence frequency, and the values of the parameters of the elastic element and the turbulent flow.

An analysis of the turbulent power distribution with respect to frequency (see Figure 5) given in section 4.2. shows that it is reasonable to consider only relatively low frequencies, where the main part of the turbulent power is contained. In addition, for efficient resonant excitation and for efficient radiation, the excited structure should be sufficiently elastic. This means that, for the frequency scale U_∞/δ^* of the flow in the turbulent boundary layer,

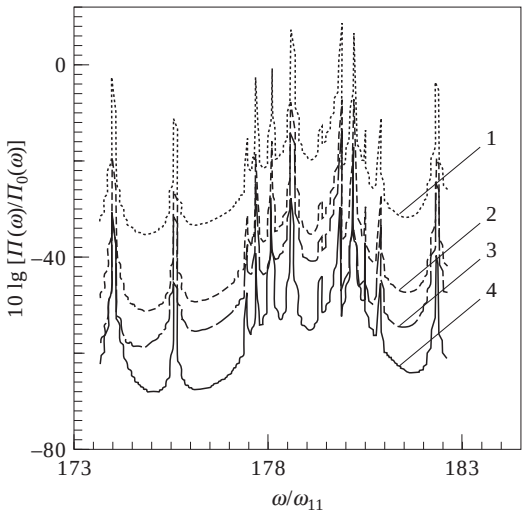

Figure 6. Sound power radiated by turbulence excited panel in air ($U_\infty = 40$ m/s) calculated for 1, the Corcos model; 2, the Ffowcs Williams model; 3, the Smol'yakov–Tkachenko model and 4, the Chase model.

the natural frequencies ω_{mn} of the plate lower modes fall in the given frequency interval. In other words, the mechanical and geometrical characteristics of the elastic element should be taken in such a way that the plate lower natural frequencies satisfy the condition $\omega\delta^*/U_\infty \approx \omega_{mn}\delta^*/U_\infty$. The case when the lower natural frequencies fall outside the mentioned interval ($\omega\delta^*/U_\infty \ll \omega_{mn}\delta^*/U_\infty$) corresponds in fact to a flow around a rigid structure and is not studied in this paper.

Under these conditions, the expression for the radiated power (52) will contain only resonances of the modes with a relatively small number of nodal lines (viz., the long wavelength modes). These modes at their resonances were shown in section 4.2. to generate much higher sound levels than do the convective modes. This fact permits one to neglect the convective mode contribution in the acoustic energy (52) radiated by the plate. Consequently, for the practically important frequency ranges of the energy containing turbulent fluctuations, the long wavelength subconvective and short wavelength convective

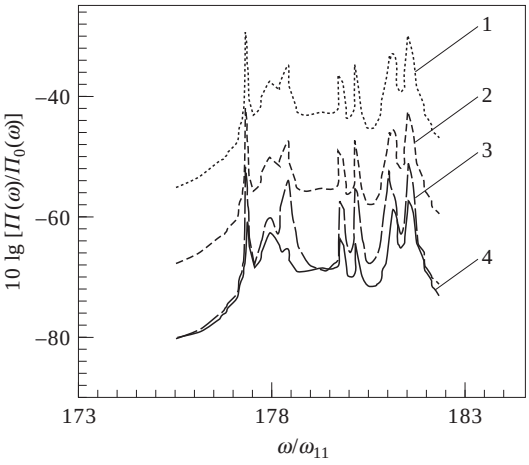

Figure 7. Sound power radiated by turbulence excited panel in water ($U_\infty = 10$ m/s) calculated for 1, the Corcos model; 2, the Ffowcs Williams model; 3, the Smol'yakov–Tkachenko model; 4, the Chase model.

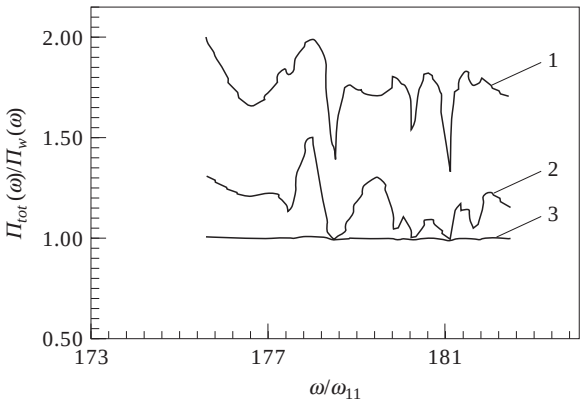

Figure 8. Ratio Π_{tot}/Π_w of the total acoustic power (with the inclusion of the convective domain contribution, $\Pi_{tot} = \Pi_{ac} + \Pi_{low\text{–}w.n.} + \Pi_{conv}$) to the acoustic power obtained without taking into account the wall pressure convective component contribution ($\Pi_w = \Pi_{ac} + \Pi_{low\text{–}w.n.}$) calculated for 1, the Chase model; 2, the Smol'yakov–Tkachenko model; 3, the Ffowcs Williams model.

wall pressure components make their contribution to the radiated sound only by exciting long wavelength modes.

The predictions of the radiated acoustic power (52), as calculated with use of the turbulent wall pressure models considered, are shown in Figures 6 and 7. The calculations of the quantity $10 \lg [\Pi(\omega)/\Pi_0(\omega)]$ (where $\Pi_0(\omega) = l_1 l_2 \rho_0 c_0 P(\omega)/4m_s^2\omega^2$) were performed below the plate coincidence frequency, the choice of the frequency range being correlated with the above reasoning about relatively low frequencies in the power spectrum $P(\omega)$. Therefore, both the high-efficiency nonresonant modes ($\sigma_{mn} \approx 1$, $\omega \neq \omega_{mn}$) and low-efficiency resonant modes ($\sigma_{mn} \ll 1$, $\omega \approx \omega_{mn}$) were taken into account [16, 24]. It should be stressed that all the modes chosen were the long wavelength modes.

In the calculations, the plate parameters were taken as $l_1 = 0{\cdot}6$ m, $l_2 = 0{\cdot}4$ m, $h = 0{\cdot}001$ m, $\rho_s = 2770$ kg/m^3 and $E = 7 \times 10^{10}$ N/m^2, and the frequencies were normalized by the plate lowest natural frequency ω_{11}. The radiation was assumed to be into light (air, Figure 6; $U_\infty = 40$ m/s) and heavy (water, Figure 7; $U_\infty = 10$ m/s) acoustic media. In air, the influence of the added mass m_{mn} on the *in vacuo* resonance frequency ω_{mn} was neglected, and the total damping $\eta_s + \rho_0 c_0 \sigma_{mn}(\omega)/m_s\omega$ was considered to be dominated by the structural damping η_s. In water, in the vicinity of the resonances $\omega_{mn}/(1 + m_{mn}/m_s)^{1/2}$, the flux of the acoustic energy is controlled by the radiation damping $\rho_0 c_0 \sigma_{mn}(\omega)/m_s\omega$.

One can notice the differences between the predictions of the radiated acoustic power for the various wall pressure models. These differences are practically constant, though the radiation levels strongly depend on frequency. The above analysis of expression (52) allows us to conclude that the differences are due to the different magnitudes of the excitation term $\Phi_{p_{mn}}(\omega)$ in the different models. All resonances shown in Figures 6 and 7 are identified with the plate natural frequencies, which are contained in the structural response term a_{mn}.

The calculations show that in the case of the Corcos and Ffowcs Williams models the contribution of the convective range of the spectrum $\Phi_p(k_1, k_2, \omega)$ to the low Mach number turbulent energy re-emitted by the plate is negligible in comparison to that of the acoustic and low-wavenumber domains. That is, the total acoustic power radiated by the turbulence excited plate is dominated by the long wavelength subconvective components of the wall pressure field. However, this is not the case for the Chase and Smol'yakov–Tkachenko models. In the framework of the Chase model the convective wall pressure components are very significant. Their role can be seen from Figure 8 where the ratio of the total acoustic power (with the inclusion of the convective domain, viz.,

$\Pi(\omega)_{tot} = \Pi(\omega)_{ac} + \Pi(\omega)_{low\text{–}w.n.} + \Pi(\omega)_{conv}$) to the acoustic power obtained without taking into account the convective components ($\Pi(\omega)_w = \Pi(\omega)_{ac} + \Pi(\omega)_{low\text{–}w.n.}$) is presented. One can see that neglect of the convective domain can result in approximately a two-fold underestimation of the total acoustic power emitted.

In the Smol'yakov–Tkachenko model, the contribution of the convective components falls in the ranges 20–50% of the long wavelength component contribution depending on frequency.

6. CONCLUSIONS

The primary results of this paper are as follows.

1. In this study the Corcos, Chase, Ffowcs Williams and Smol'yakov–Tkachenko incompressible turbulent wall pressure models were used. The comparative analysis of the models was carried out in order to determine which of them are preferable for theoretical predictions of vibration and acoustic fields of elastic structures excited by low Mach number turbulence. For the conditions considered in this work, these are the Chase and Smol'yakov–Tkachenko models.

2. The contribution of the wall pressure convective components in the vibration and acoustic fields of elastic elements excited by low Mach number turbulence was shown to be significant for the Chase and Smol'yakov–Tkachenko models. Associated with taking into account the convective components, the effects of turbulent energy conversion on structural inhomogeneities (e.g., on a plate supported edge) cause a considerable increase in the energy radiated.

3. The ranges of the parameter values of a flow and elastic structure were found (away from structural resonances) for which the differences between the wall pressure models are not important for predictions of sound radiated. This is due to the fact that in this case the radiated acoustic power is dominated by the convective components, which are identically described by the models. At the same time the differences between the models are important near structural resonances, because in these domains the main contribution to the radiated acoustic power comes from the long wavelength subconvective components.

4. The differences in the predictions of the sound field produced by turbulence excited elastic rectangular plate in both light (air) and heavy (water) acoustic media have been demonstrated. The differences are caused by the differences in the models of the wall pressure wavenumber–frequency spectrum.

ACKNOWLEDGMENTS

The authors gratefully acknowledge the financial support of the State Committee of Ukraine for Science and Technology. We also thank the referees for a number of constructive comments which have helped us to improve the paper.

REFERENCES

1. W. K. Blake 1986 *Mechanics of Flow-Induced Sound and Vibration* (two volumes). New York: Academic Press.
2. E. H. Dowell 1975 *Aeroelasticity of Plates and Shells*. Leyden, The Netherlands: Noordhoff International.
3. G. M. Corcos 1963 *Journal of the Acoustical Society of America* **35**, 192–199. The resolution of pressure in turbulence.

4. N. C. Martin and P. Leehey 1977 *Journal of Sound and Vibration* **52**, 95–120. Low wavenumber wall pressure measurements using a rectangular membrane as a spatial filter.
5. O. M. Phillips 1956 *Proceedings of the Royal Society of London* **A234**, 327–335. On the aerodynamic surface sound from a plane turbulent boundary layer.
6. R. H. Kraichnan 1956 *Journal of the Acoustical Society of America* **28**, 378–390. Pressure fluctuations in a turbulent flow over a flat plate.
7. M. S. Howe 1992 *Journal of Fluid Mechanics* **234**, 443–448. A note on the Kraichnan–Phillips theorem.
8. D. M. Chase 1980 *Journal of Sound and Vibration* **70**, 29–67. Modelling the wavevector–frequency spectrum of turbulent boundary layer wall pressure.
9. J. E. Ffowcs Williams 1982 *Journal of Fluid Mechanics* **125**, 9–25. Boundary-layer pressures and the Corcos model: a development to incorporate low-wavenumber constraints.
10. A. V. Smol'yakov and V. M. Tkachenko 1991 *Akusticheskii Zhurnal* **37**, 1199–1207. Models of pseudosound turbulent wall pressure field and experimental data (in Russian).
11. Y. F. Hwang and F. E. Geib 1983 *Proceedings of the International Symposium on Turbulence-Induced Vibrations and Noise of Structures*, *Boston*, 13–18 *Nov*. 13–30: Estimation of wavevector-frequency spectrum of turbulent boundary layer wall pressure by multiple linear regression.
12. R. H. Mellen 1994 *Journal of the Acoustical Society of America* **95**, 1671–1673. Wavevector filter analysis of turbulent flow.
13. D. G. Crighton 1983 *Proceedings of the International Symposium on Turbulence-Induced Vibrations and Noise of Structures*, *Boston*, 13–18 *Nov*. 107–123: Long range acoustic scattering by surface inhomogeneities beneath a turbulent boundary layer.
14. M. J. Lighthill 1952 *Proceedings of the Royal Society of London* **A211**, 564–587. On sound generated aerodynamically. 1. General theory.
15. M. J. Lighthill 1954 *Proceedings of the Royal Society of London* **A221**, 1–32. On sound generated aerodynamically. 2. Turbulence as a source of sound.
16. A. A. Borisyuk 1993 *Ph.D. Thesis*, *Institute of Hydromechanics*, *Kiev*, *Ukraine*. Vibration and sound radiation by elastic plates excited by turbulent flow. (in Russian).
17. V. T. Grinchenko and A. A. Borisyuk 1993 *Hydromechanics* **66**, 24–28. Comparative analysis of models for the pressure fluctuation field beneath turbulent boundary layer (in Russian).
18. M. C. Junger and D. Feit 1972 *Sound*, *Structures and Their Interaction*. Cambridge, Massachusetts: M.I.T. Press.
19. A. A. Borisyuk 1994 *Akusticheskii Zhurnal* **40**, 903–908. Acoustic radiation of an elastic rectangular plate excited by a turbulent boundary layer (in Russian).
20. W. R. Graham 1993 *Ph.D. Thesis*, *Cambridge University*, *Engineering Department*, *Cambridge*, *England*. Boundary-layer noise and vibration.
21. W. R. Graham 1995 *Philosophical Transactions of the Royal Society of London* **A352**, 1–43. High-frequency vibration and acoustic radiation of fluid-loaded plates.
22. H. G. Davies 1971 *Journal of the Acoustical Society of America* **49**, 878–889. Sound from turbulent-boundary-layer-excited panels.
23. H. G. Davies 1971 *Journal of Sound and Vibration* **15**, 107–126. Low frequency random excitation of water-loaded rectangular plates.
24. F. G. Leppington, E. G. Broadbent, K. H. Heron and S. M. Mead 1986 *Proceedings of the Royal Society of London* **A406**, 139–171. Resonant and non-resonant acoustic properties of elastic panels. 1. The radiation problem.

APPENDIX: LIST OF SYMBOLS

(x_1, x_2, x_3), (x, y, z)	Cartesian rectangular co-ordinates
ξ_1, ξ_2	space separations in the streamwise and the crossflow directions, respectively.
t, τ	time and time delay, respectively
ω	circular frequency
k_1, k_2	wavenumbers in the flow and the crossflow directions, respectively
k	wavenumber in the flow direction
l_1, l_2	streamwise and crossflow dimensions (length and width) of either membrane or plate, respectively
l	width of strip
h	height of either plate or strip

ρ_s	mass density of either strip or plate
ρ_0	mass density of acoustic medium
m_s	mass per unit area of either membrane or strip or plate
D_s	bending stiffness of either strip or plate
E	Young's modulus
v	Poisson's ratio
β	damping coefficient of either membrane or plate
η_s	loss factor in either membrane or plate material
T	membrane uniform tensile force per unit length
Ψ_{mn}	normal modes of either membrane or plate
Ψ_m	normal modes of strip
ω_{mn}	*in vacuo* natural frequencies of either membrane or plate
ω_j	*in vacuo* natural frequencies of strip
c	*in vacuo* membrane wave speed
c_p	bending wave speed in either strip or plate material
w	membrane normal displacement
v	normal velocity of either strip or plate
k_m, k_n, k_s	structural wavenumbers
α_j	wavenumbers
V, V_j	strip's modal velocity amplitudes
V_{mn}	plate modal velocity amplitudes
P, P_j	strip's wall pressure amplitudes
σ_j	radiation efficiency coefficient of the strip's jth normal mode
σ_{mn}	radiation efficiency coefficient of the (m, n)th normal mode of plate
m_j	specific added mass of the strip's jth normal mode
m_{mn}	specific added mass of the (m, n)th normal mode of plate
Z_{mnrs}	plate modal impedances
Z_{mnmn}	plate radiation modal impedances
$\lvert A_m(k_1)\rvert^2, \lvert A_n(k_2)\rvert^2$	shape functions of either membrane or plate
$\lvert A_j(k)\rvert^2$	shape functions of strip
a_{mn}	structural response term
$\lvert H_{mn}\rvert^2$	term which describes the membrane frequency response
$\Phi_{p_{mn}}$	modal excitation term
U_∞	free stream velocity
U_c	convective velocity
v_*	friction velocity
c_0	sound speed in acoustic medium
M	Mach number
M_c	convective Mach number
λ_0	acoustic wavelength
k_0	acoustic wavenumber
k_c	convective wavenumber
δ	boundary layer thickness
$\delta( )$	Dirac delta function
Δ	boundary layer thickness in the Ffowcs Williams model
δ_*	boundary layer displacement thickness
τ_w	wall shear stress
p_t	turbulent wall pressure
p_0	acoustic pressure
R_p	space-time cross correlation function of turbulent wall pressure
S_p	cross spectral density of turbulent wall pressure
Φ_p	wavenumber-frequency spectrum of turbulent wall pressure
P	power (frequency) spectrum of turbulent wall pressure
S_w	membrane response spectral density
Π	power spectrum of acoustic field produced by either strip or plate